

Electromagnetic Negative–Phase–Velocity Propagation in the Ergosphere of a Rotating Black Hole

Tom G. Mackay*

School of Mathematics, University of Edinburgh, Edinburgh EH9 3JZ, UK

Akhlesh Lakhtakia†

Department of Engineering Science and Mechanics

Pennsylvania State University, University Park, PA 16802–6812, USA

Sandi Setiawan‡

School of Mathematics, University of Edinburgh, Edinburgh EH9 3JZ, UK

Abstract

We report on the occurrence of negative–phase velocity (NPV) planewave propagation in the ergosphere of a rotating black hole. By implementing the Kerr metric, it is demonstrated that regions of NPV propagation are concentrated at the equator of the ergosphere, while NPV propagation is less common towards the polar regions. Increasing the angular velocity of the black hole exaggerates the NPV concentration at the equator. NPV propagation is not observed outside the stationary limit surface.

Keywords: General theory of relativity, Negative phase velocity, Poynting vector, Kerr spacetime

1 Introduction

The term *negative–phase velocity* (NPV) refers to a mode of electromagnetic planewave propagation in which the phase velocity vector is directed opposite to the direction of time–averaged energy flux [1, 2]. Of the many interesting consequences of NPV propagation, it is the phenomenon of negative refraction which has recently attracted much attention in the electromagnetics/optics and materials research communities [3]. This interest may be traced back to the first experimental reports of negative refraction in 2001, involving the microwave illumination of an artificial *metamaterial* [4].

We have recently begun to examine the possibility of gravitationally–assisted NPV propagation in vacuum [5, 6]. In the absence of a ‘material’, the source of the NPV may be

*Corresponding Author. Fax: + 44 131 650 6553; e–mail: T.Mackay@ed.ac.uk.

†Corresponding Author. Fax: +1 814 863 4319; e–mail: akhlesh@psu.edu; also affiliated with Department of Physics, Imperial College, London SW7 2 BZ, UK

‡Fax: + 44 131 650 6553; e–mail: S.Setiawan@ed.ac.uk.

provided by the curvature of spacetime. The electrodynamic formulation adopted is founded on the formal analogy between (a) electromagnetic propagation in curved spacetime in free space; and (b) electromagnetic propagation in flat spacetime in a fictitious, instantaneously responding bianisotropic medium. This approach — which was originally put forward by Tamm and subsequently described by numerous authors [7]–[13] — enables wave propagation in curved spacetime to be examined using standard electromagnetic techniques. Thereby, the feasibility of NPV propagation for a general gravitomagnetic metric has been established [14].

We further develop the concept of gravitationally–assisted NPV propagation in this paper with a detailed numerico–theoretical study based on a particular gravitomagnetic metric, namely the Kerr metric [15]. Specifically, we explore the spacetime surrounding a rotating black hole, in search of regions where NPV propagation occurs. Our search is restricted to the physically probeable spacetime outside the outer event horizon. The theoretical framework is described in Section 2, numerical results are presented and analyzed in Section 3, and conclusions are itemized and discussed in Section 4.

2 Theoretical framework

The electrodynamics of the classical vacuum in a curved spacetime provides the setting for our numerico–theoretical study. Thus, we consider the covariant and the contravariant electromagnetic field tensors $f_{\alpha\beta}$ and $h^{\alpha\beta}$, respectively, which appear in the source–free covariant Maxwell equations[§]

$$\left. \begin{aligned} f_{\alpha\beta;\nu} + f_{\beta\nu;\alpha} + f_{\nu\alpha;\beta} &= 0 \\ h^{\alpha\beta}{}_{;\beta} &= 0 \end{aligned} \right\}, \quad (1)$$

where the subscript ${}_{;\nu}$ indicates the covariant derivative with respect to the ν th spacetime coordinate x^ν . The spacetime curvature is described by the metric $g_{\alpha\beta}$ with signature $(+, -, -, -)$.

2.1 Electrodynamic formulation

We follow the standard approach [8]–[11] — originally proposed by Tamm — wherein the covariant equations (1) are replaced by their noncovariant equivalents

$$\left. \begin{aligned} f_{\alpha\beta,\nu} + f_{\beta\nu,\alpha} + f_{\nu\alpha,\beta} &= 0 \\ \left[(-g)^{1/2} h^{\alpha\beta} \right]_{;\beta} &= 0 \end{aligned} \right\}, \quad (2)$$

[§]Greek indexes take the values 0, 1, 2 and 3; Roman indexes take the values 1, 2 and 3; $x^0 = ct$ where c is the speed of light in vacuum in the absence of all gravitational fields; whereas $x^{1,2,3}$ are the three spatial coordinates.

with $g = \det [g_{\alpha\beta}]$ and the subscript $_{,\nu}$ denoting ordinary differentiation with respect to the ν th spacetime coordinate. More conveniently, we express (2) in the familiar form

$$\left. \begin{aligned} B_{\ell,\ell} &= 0, & B_{\ell,0} + \varepsilon_{\ell mn} E_{m,n} &= 0 \\ D_{\ell,\ell} &= 0, & -D_{\ell,0} + \varepsilon_{\ell mn} H_{m,n} &= 0 \end{aligned} \right\}, \quad (3)$$

where $\varepsilon_{\ell mn}$ is the three-dimensional Levi-Civita symbol. The conventional electromagnetic field vectors \underline{E} , \underline{B} , \underline{D} and \underline{H} are the 3 vector-equivalents associated with the respective components

$$\left. \begin{aligned} E_\ell &= f_{\ell 0}, \\ B_\ell &= (1/2)\varepsilon_{\ell mn} f_{mn} \\ D_\ell &= (-g)^{1/2} h^{\ell 0}, \\ H_\ell &= (1/2)\varepsilon_{\ell mn} (-g)^{1/2} h^{mn} \end{aligned} \right\} \quad (4)$$

introduced in (3). Thus, in (3), $B_{\ell,\ell}$ and $D_{\ell,\ell}$ represent the divergences of \underline{B} and \underline{D} , whereas the ℓ th vector component of the curls of \underline{E} and \underline{H} are represented as $\varepsilon_{\ell mn} E_{m,n}$ and $\varepsilon_{\ell mn} H_{m,n}$, with the derivatives with respect to time of the ℓ th vector component of \underline{B} and \underline{D} being represented as $B_{\ell,0}$ and $D_{\ell,0}$. The electromagnetic field vector components satisfy the constitutive relations

$$\left. \begin{aligned} D_\ell &= \gamma_{\ell m} E_m + \varepsilon_{\ell mn} \Gamma_m H_n \\ B_\ell &= \gamma_{\ell m} H_m - \varepsilon_{\ell mn} \Gamma_m E_n \end{aligned} \right\}, \quad (5)$$

where the tensor $\gamma_{\ell m}$ components and vector Γ_m components are defined as

$$\left. \begin{aligned} \gamma_{\ell m} &= -(-g)^{1/2} \frac{g^{\ell m}}{g_{00}} \\ \Gamma_m &= \frac{g_{0m}}{g_{00}} \end{aligned} \right\}. \quad (6)$$

Thus, in terms of the noncovariant formulation (2), vacuum is represented by the fictitious, instantaneously-responding, bianisotropic medium characterized by (5).

For later use, we recast (3) and (5) in 3×3 dyadic/ 3 vector form as

$$\left. \begin{aligned} \nabla \times \underline{E}(ct, \underline{r}) + \frac{\partial}{\partial t} \underline{B}(ct, \underline{r}) &= 0 \\ \nabla \times \underline{H}(ct, \underline{r}) - \frac{\partial}{\partial t} \underline{D}(ct, \underline{r}) &= 0 \end{aligned} \right\} \quad (7)$$

and

$$\left. \begin{aligned} \underline{D}(ct, \underline{r}) &= \epsilon_0 \underline{\underline{\gamma}}(ct, \underline{r}) \cdot \underline{E}(ct, \underline{r}) - \frac{1}{c} \underline{\Gamma}(ct, \underline{r}) \times \underline{H}(ct, \underline{r}) \\ \underline{B}(ct, \underline{r}) &= \mu_0 \underline{\underline{\gamma}}(ct, \underline{r}) \cdot \underline{H}(ct, \underline{r}) + \frac{1}{c} \underline{\Gamma}(ct, \underline{r}) \times \underline{E}(ct, \underline{r}) \end{aligned} \right\}, \quad (8)$$

respectively, wherein $\underline{\underline{\gamma}}(ct, \underline{r})$ is the dyadic-equivalent of $\gamma_{\ell m}$, $\underline{\Gamma}(ct, \underline{r})$ is the vector-equivalent of Γ_m ; the scalar constants ϵ_0 and μ_0 denote the permittivity and permeability of vacuum in

the absence of a gravitational field; and SI units are adopted. In moving from (1) to (7) and (8), the spacetime coordinate x^α has been separated into space \underline{r} and time t coordinates. The vector cross products and dyadic–vector dot products in (7) and (8) apply to vectors and dyadics associated with the three spatial dimensions of flat spacetime [16]. However, it is emphasized that the spacetime underlying (7) and (8) remains curved.

2.2 Kerr spacetime

We consider a specific gravitomagnetic spacetime, namely the Kerr spacetime [15], which describes a rotating black hole. In Cartesian coordinates — $\underline{r} \equiv (x, y, z)$ — the components of the Kerr metric are given as [17]

$$g_{00} = 1 - \Delta, \quad (9)$$

$$g_{01} = -\Delta \frac{Rx + a_{\text{rbh}}y}{R^2 + a_{\text{rbh}}^2}, \quad (10)$$

$$g_{02} = -\Delta \frac{Ry - a_{\text{rbh}}x}{R^2 + a_{\text{rbh}}^2}, \quad (11)$$

$$g_{03} = -\Delta \frac{z}{R}, \quad (12)$$

$$g_{11} = -1 - \Delta \left(\frac{Rx + a_{\text{rbh}}y}{R^2 + a_{\text{rbh}}^2} \right)^2, \quad (13)$$

$$g_{12} = -\Delta \frac{(Rx + a_{\text{rbh}}y)(Ry - a_{\text{rbh}}x)}{(R^2 + a_{\text{rbh}}^2)^2}, \quad (14)$$

$$g_{13} = -\Delta \frac{(Rx + a_{\text{rbh}}y)z}{(R^2 + a_{\text{rbh}}^2)R}, \quad (15)$$

$$g_{22} = -1 - \Delta \left(\frac{a_{\text{rbh}}x - Ry}{R^2 + a_{\text{rbh}}^2} \right)^2, \quad (16)$$

$$g_{23} = -\Delta \frac{(Ry - a_{\text{rbh}}x)z}{(R^2 + a_{\text{rbh}}^2)R}, \quad (17)$$

$$g_{33} = -1 - \Delta \left(\frac{z}{R} \right)^2, \quad (18)$$

with $g_{\alpha\beta} = g_{\beta\alpha}$. The quantity R is given implicitly via

$$R^2 = x^2 + y^2 + z^2 - a_{\text{rbh}}^2 \left[1 - \left(\frac{z}{R} \right)^2 \right]; \quad (19)$$

also,

$$\Delta = \frac{2m_{\text{rbh}}R^3}{R^4 + (a_{\text{rbh}}z)^2}. \quad (20)$$

The components (9)–(18) of the metric describe a black hole of geometric mass m_{rbh} , rotating about the Cartesian z axis, in conventional units. The term a_{rbh} is a measure of the black hole’s angular velocity (sometimes referred to as the specific angular momentum).

We note that the Kerr metric is often represented in terms of Boyer–Lindquist coordinates [17, Sec. 19.3]. However, for the planewave analysis undertaken in the following sections, the Cartesian representation (9)–(18) is more convenient.

Using the definitions (6) together with (9)–(18), we obtain

$$\gamma_{11} = \delta [R^4 + (a_{\text{rbh}}z)^2] \left[1 - \Delta \left(\frac{Rx + a_{\text{rbh}}y}{R^2 + a_{\text{rbh}}^2} \right)^2 \right], \quad (21)$$

$$\gamma_{12} = -2\delta m_{\text{rbh}} R^3 \frac{(Rx + a_{\text{rbh}}y)(Ry - a_{\text{rbh}}x)}{(R^2 + a_{\text{rbh}}^2)^2} \quad (22)$$

$$\gamma_{13} = -2\delta m_{\text{rbh}} R^2 z \frac{Rx + a_{\text{rbh}}y}{R^2 + a_{\text{rbh}}^2} \quad (23)$$

$$\gamma_{22} = \delta [R^4 + (a_{\text{rbh}}z)^2] \left[1 - \Delta \left(\frac{a_{\text{rbh}}x - Ry}{R^2 + a_{\text{rbh}}^2} \right)^2 \right], \quad (24)$$

$$\gamma_{23} = -2\delta m_{\text{rbh}} R^2 z \frac{Ry - a_{\text{rbh}}x}{R^2 + a_{\text{rbh}}^2} \quad (25)$$

$$\gamma_{33} = \delta [R^4 + (a_{\text{rbh}}z)^2] \left[1 - \Delta \left(\frac{z}{R} \right)^2 \right], \quad (26)$$

with $\gamma_{\ell m} = \gamma_{m\ell}$, and

$$\Gamma_1 = -2\delta m_{\text{rbh}} R^3 \left(\frac{Rx + a_{\text{rbh}}y}{R^2 + a_{\text{rbh}}^2} \right), \quad (27)$$

$$\Gamma_2 = -2\delta m_{\text{rbh}} R^3 \left(\frac{Ry - a_{\text{rbh}}x}{R^2 + a_{\text{rbh}}^2} \right), \quad (28)$$

$$\Gamma_3 = -2\delta m_{\text{rbh}} R^2 z, \quad (29)$$

wherein

$$\delta = \frac{1}{R^4 + (a_{\text{rbh}}z)^2 - 2m_{\text{rbh}}R^3}. \quad (30)$$

We concentrate on the regime $m_{\text{rbh}}^2 > a_{\text{rbh}}^2$. Furthermore, as our interest lies in physically observable phenomena, we restrict attention to the region $R > R_+$ where

$$R_+ = m_{\text{rbh}} + \sqrt{m_{\text{rbh}}^2 - a_{\text{rbh}}^2} \quad (31)$$

represents the outer event horizon of the black hole. Finally, we note that $R_+ \leq R_{S_+}$ where

$$R_{S_+} = m_{\text{rbh}} + \sqrt{m_{\text{rbh}}^2 - \left(\frac{a_{\text{rbh}}z}{R_{S_+}} \right)^2} \quad (32)$$

delineates the stationary limit surface of the black hole.

2.3 Planewave propagation

Let us consider the propagation of plane waves in the medium characterized by the constitutive relations (8). Our strategy is to focus upon an arbitrary neighbourhood \mathcal{R} whose location is specified by the Cartesian coordinates $(\tilde{x}, \tilde{y}, \tilde{z})$. The neighbourhood is presumed to be sufficiently small that the nonuniform metric $g_{\alpha\beta}$ may be approximated by the uniform metric $\tilde{g}_{\alpha\beta}$ throughout \mathcal{R} . Thus, within \mathcal{R} , the uniform 3×3 dyadic $\tilde{\underline{\underline{\gamma}}} \equiv \underline{\underline{\gamma}}|_{\mathcal{R}}$ plays the role of the metric with components (21)–(26), whereas the uniform 3 vector $\tilde{\underline{\underline{\Gamma}}} \equiv \underline{\underline{\Gamma}}|_{\mathcal{R}}$ plays the role of the vector with components (27)–(29). As a consequence of the uniform metric approximation, henceforth we restrict our consideration to electromagnetic wavelengths which are small compared with the linear dimensions of the neighbourhood \mathcal{R} .

Within the neighbourhood \mathcal{R} , the electromagnetic fields are decomposed via the three-dimensional Fourier transforms

$$\left. \begin{aligned} \underline{\underline{E}}(ct, \underline{\underline{r}}) &= \frac{1}{c} \int_{-\infty}^{\infty} \int_{-\infty}^{\infty} \int_{-\infty}^{\infty} \underline{\underline{E}}(\omega/c, \underline{\underline{k}}) \exp[i(\underline{\underline{k}} \cdot \underline{\underline{r}} - \omega t)] d\omega dk_1 dk_2 \\ \underline{\underline{H}}(ct, \underline{\underline{r}}) &= \frac{1}{c} \int_{-\infty}^{\infty} \int_{-\infty}^{\infty} \int_{-\infty}^{\infty} \underline{\underline{H}}(\omega/c, \underline{\underline{k}}) \exp[i(\underline{\underline{k}} \cdot \underline{\underline{r}} - \omega t)] d\omega dk_1 dk_2 \end{aligned} \right\}, \quad (33)$$

where the wavevector $\underline{\underline{k}}$ is the Fourier variable corresponding to $\underline{\underline{r}}$, $i = \sqrt{-1}$ and ω is the usual temporal frequency. The wavevector component k_3 is determined by combining (33) with the Maxwell curl postulates (7) and then solving the resulting 4×4 eigenvalue problem [18]. We take $k_3 \in \mathbb{R}$ and thereby consider only propagating (non-evanescent) plane waves.

The associated rate of energy flow is calculated from the complex-valued phasors of the electric and magnetic fields, $\underline{\underline{E}}(\omega/c, \underline{\underline{k}})$ and $\underline{\underline{H}}(\omega/c, \underline{\underline{k}})$ respectively, by means of the time-averaged Poynting vector[¶]

$$\langle \underline{\underline{P}}(\omega/c, \underline{\underline{k}}) \rangle_t = \frac{1}{2} \operatorname{Re} \{ \underline{\underline{E}}(\omega/c, \underline{\underline{k}}) \times \underline{\underline{H}}^*(\omega/c, \underline{\underline{k}}) \}. \quad (34)$$

If the phase velocity vector casts a negative projection onto the time-averaged Poynting vector then we have so-called negative phase velocity (NPV); i.e., NPV is signalled by

$$\underline{\underline{k}} \cdot \langle \underline{\underline{P}}(\omega/c, \underline{\underline{k}}) \rangle_t < 0. \quad (35)$$

The key steps involved in deriving a general expression for the quantity $\underline{\underline{k}} \cdot \langle \underline{\underline{P}}(\omega/c, \underline{\underline{k}}) \rangle_t$ follow the corresponding steps for a simply moving medium which is isotropic dielectric-magnetic at rest [16], [19]. We begin by combining the Fourier decompositions (33) with the constitutive relations (8) and the Maxwell curl postulates (7). Thereby, we find

$$\underline{\underline{p}} \times \underline{\underline{E}}(\omega/c, \underline{\underline{k}}) = \omega \mu_0 \tilde{\underline{\underline{\gamma}}} \cdot \underline{\underline{H}}(\omega/c, \underline{\underline{k}}), \quad (36)$$

$$\underline{\underline{p}} \times \underline{\underline{H}}(\omega/c, \underline{\underline{k}}) = -\omega \epsilon_0 \tilde{\underline{\underline{\gamma}}} \cdot \underline{\underline{E}}(\omega/c, \underline{\underline{k}}) \quad (37)$$

[¶] $\operatorname{Re}\{\cdot\}$ denotes the real part while the asterisk denotes the complex conjugate.

where the vector

$$\underline{p} = \underline{k} - \frac{\omega}{c} \underline{\tilde{\Gamma}} \quad (38)$$

has been introduced. Upon substituting (36) into (37) and carrying out some algebraic manipulations, we obtain the eigenvector equation

$$\left\{ \left[\left(\frac{\omega}{c} \right)^2 |\underline{\tilde{\gamma}}| - \underline{p} \cdot \underline{\tilde{\gamma}} \cdot \underline{p} \right] \underline{I} + \underline{p} \underline{p} \cdot \underline{\tilde{\gamma}} \right\} \cdot \underline{\mathbf{E}}(\omega/c, \underline{k}) = \underline{0} \quad (39)$$

and the corresponding dispersion relation

$$\left[\underline{p} \cdot \underline{\tilde{\gamma}} \cdot \underline{p} - \left(\frac{\omega}{c} \right)^2 |\underline{\tilde{\gamma}}| \right]^2 = 0. \quad (40)$$

Here, \underline{I} is the identity dyadic, and $|\underline{\tilde{\gamma}}|$ denotes the determinant of $\underline{\tilde{\gamma}}$.

To solve (39), we exploit the orthogonality condition

$$\underline{p} \cdot \underline{\tilde{\gamma}} \cdot \underline{\mathbf{E}}(\omega/c, \underline{k}) = 0. \quad (41)$$

which follows from (40). The general solution to the electric phasor equation (39) is expressible as the sum

$$\underline{\mathbf{E}}(\omega/c, \underline{k}) = A_a(\omega/c, \underline{k}) \underline{\mathbf{e}}_a(\omega/c, \underline{k}) + A_b(\omega/c, \underline{k}) \underline{\mathbf{e}}_b(\omega/c, \underline{k}) \quad (42)$$

where the unit vectors

$$\left. \begin{aligned} \underline{\mathbf{e}}_a &= \frac{\underline{\tilde{\gamma}}^{-1} \cdot \underline{w}}{|\underline{\tilde{\gamma}}^{-1} \cdot \underline{w}|} \\ \underline{\mathbf{e}}_b &= \frac{\underline{\tilde{\gamma}}^{-1} \cdot (\underline{p} \times \underline{\mathbf{e}}_a)}{|\underline{\tilde{\gamma}}^{-1} \cdot (\underline{p} \times \underline{\mathbf{e}}_a)|} \end{aligned} \right\}. \quad (43)$$

are chosen in accordance with (41). The unit vector \underline{w} is orthogonal to \underline{p} , i.e., $\underline{w} \cdot \underline{p} = 0$, but is otherwise arbitrary. For calculating the numerical results presented in the following section, we chose

$$\underline{w} = \begin{cases} \frac{1}{\sqrt{2p_z^2 + (p_x + p_y)^2}} (p_z, p_z, -p_x - p_y) & \text{for } p_z \neq 0 \\ \frac{1}{\sqrt{p_y^2 + p_x^2}} (p_y, -p_x, 0) & \text{for } p_z = 0 \end{cases}, \quad (44)$$

with $\underline{p} \equiv (p_x, p_y, p_z)$ in the Cartesian coordinate system. Initial and boundary conditions fix the complex-valued amplitudes $A_{a,b}(\omega/c, \underline{k})$. The general solution to the magnetic phasor equation corresponding to (39) follows directly from (42) upon substitution into (36).

Finally, combining (39) and (36) yields the central result

$$\underline{k} \cdot \langle \underline{\mathbf{P}} \rangle_t = \frac{1}{2\omega\mu_0|\underline{\tilde{\gamma}}|} \left(|A_a|^2 \underline{\mathbf{e}}_a \cdot \underline{\tilde{\gamma}} \cdot \underline{\mathbf{e}}_a + |A_b|^2 \underline{\mathbf{e}}_b \cdot \underline{\tilde{\gamma}} \cdot \underline{\mathbf{e}}_b \right) \underline{k} \cdot \underline{\tilde{\gamma}} \cdot \underline{p}. \quad (45)$$

For the Kerr metric, we observe that

$$|\underline{\tilde{\gamma}}| = \delta^2 [R^4 + (a_{\text{rbh}}z)^2]^2. \quad (46)$$

Therefore, it follows that $|\underline{\tilde{\gamma}}| > 0$ and the sufficient condition

$$\left. \begin{array}{l} P_a < 0 \\ P_b < 0 \end{array} \right\} \quad (47)$$

for NPV propagation arises, wherein

$$\left. \begin{array}{l} P_a = \left(\underline{\mathbf{e}}_a \cdot \underline{\tilde{\gamma}} \cdot \underline{\mathbf{e}}_a \right) \left(\underline{k} \cdot \underline{\tilde{\gamma}} \cdot \underline{p} \right) \\ P_b = \left(\underline{\mathbf{e}}_b \cdot \underline{\tilde{\gamma}} \cdot \underline{\mathbf{e}}_b \right) \left(\underline{k} \cdot \underline{\tilde{\gamma}} \cdot \underline{p} \right) \end{array} \right\}. \quad (48)$$

The dispersion relation (40) yields two wavenumbers $k = k^\pm$ for the arbitrarily oriented wavevector $\underline{k} = k\hat{\underline{k}}$ with $\hat{\underline{k}} = (\sin\theta \cos\phi, \sin\theta \sin\phi, \cos\theta)$. These are

$$k^\pm = \frac{\omega}{c} \left(\frac{\hat{\underline{k}} \cdot \underline{\tilde{\gamma}} \cdot \hat{\underline{\Gamma}} \pm \sqrt{\left(\hat{\underline{k}} \cdot \underline{\tilde{\gamma}} \cdot \hat{\underline{\Gamma}} \right)^2 - \hat{\underline{k}} \cdot \underline{\tilde{\gamma}} \cdot \hat{\underline{k}} \left(\hat{\underline{\Gamma}} \cdot \underline{\tilde{\gamma}} \cdot \hat{\underline{\Gamma}} - |\underline{\tilde{\gamma}}| \right)}}{\hat{\underline{k}} \cdot \underline{\tilde{\gamma}} \cdot \hat{\underline{k}}} \right). \quad (49)$$

As only propagating (non-evanescent) plane waves are considered here, we have $k^\pm \in \mathbb{R}$. In order to establish whether $\underline{k} \cdot \langle \underline{\mathbf{P}} \rangle_t < 0$ for the wavenumbers k^\pm , we resort to numerical evaluations of (45) and (49).

3 Numerical results

The prospects for NPV propagation are investigated within the gravitational field of a rotating black hole, as characterized by the Kerr metric, by calculating $P_{a,b}$ of (48) for all directions of wave propagation in a chosen \mathcal{R} .

For compact presentation of our results, we considered surfaces of constant R for

$$R_+ \leq R \leq R_{S_+}. \quad (50)$$

The region represented by (50) is known as the ergosphere of the blackhole. In regions beyond the stationary limit, i.e., $R > R_{S_+}$, the NPV conditions (47) were found not to be satisfied. This observation is consistent with the asymptotic behaviour of the Kerr metric:

in the limit $R \rightarrow \infty$, Kerr spacetime converges to flat Minkowski spacetime which does not support NPV propagation in vacuum [19].

For the purposes of illustration, we chose a black hole with $a_{\text{rbh}} = m_{\text{rbh}}\sqrt{3/4}$. We explored the feasibility of NPV propagation, in all directions denoted by $\hat{\underline{k}} = (\sin \theta \cos \phi, \sin \theta \sin \phi, \cos \theta)$, at $(\tilde{x}, \tilde{y}, \tilde{z})$ neighbourhoods on surfaces of constant R . In Figure 1, the surfaces

- (a) $R = R_+$ (i.e., the outer event horizon),
- (b) $R = 0.5R_+ + 0.5R_{S_+}$,
- (c) $R = 0.25R_+ + 0.75R_{S_+}$,
- (d) $R = 0.1R_+ + 0.9R_{S_+}$, and
- (e) $R = 0.05R_+ + 0.95R_{S_+}$

are mapped for the octant $\{\tilde{x} > 0, \tilde{y} > 0, \tilde{z} > 0\}$. The three-dimensional surface mesh is constructed from \tilde{z} heights calculated on a 90×90 grid of (\tilde{x}, \tilde{y}) points. At each $(\tilde{x}, \tilde{y}, \tilde{z})$ point, the wavevector $\underline{k} = k^\pm \hat{\underline{k}}$, together with the parameters P_a and P_b , were computed at 1° increments for $\theta \in [0^\circ, 180^\circ)$ and $\phi \in [0^\circ, 360^\circ)$. If NPV was found to arise at a particular (θ, ϕ) orientation (as indicated by both $P_a < 0$ and $P_b < 0$) then the $(\tilde{x}, \tilde{y}, \tilde{z})$ grid point was given a ‘score’ of one unit.^{||} Thus, at each $(\tilde{x}, \tilde{y}, \tilde{z})$ grid point the maximum theoretical score is $180 \times 360 \times 2 = 129600$. The NPV scores are represented by colours in Figure 1. We remark that the magnitude of ω does not influence the signs of $P_{a,b}$ (nor the NPV scores).

It is clear from Figure 1 that NPV propagation is most prevalent at $(\tilde{x}, \tilde{y}, \tilde{z})$ neighbourhoods close to the equator of the outer event horizon (i.e., at neighbourhoods in the vicinity of the plane $\tilde{z} = 0$). The density of NPV propagation decreases towards the $\tilde{x} = \tilde{y} = 0$ pole of the $R = R_+$ region. We note that the ergosphere vanishes at the poles, as the outer event horizon and the stationary limit surface coincide.

For ergospheric regions outside the outer event horizon, distributions of NPV propagation density are mapped in Figure 1(b)–(e). On comparing the maps in Figure 1(a)–(e), it becomes clear that, as the constant R surfaces approach the stationary limit surface, the densities of NPV propagation become progressively more concentrated around the $\tilde{z} = 0$ equator.

In order to investigate the influence of the angular velocity term a_{rbh} we repeated the calculations of Figure 1 but with $a_{\text{rbh}} = m_{\text{rbh}}/3$. The corresponding NPV propagation maps are presented in Figure 2, for the same surfaces of constant R as were used in Figure 1. As compared with $a_{\text{rbh}} = m_{\text{rbh}}\sqrt{3/4}$, the outer event horizon and the stationary limit surface are closer together for $a_{\text{rbh}} = m_{\text{rbh}}/3$. The concentration of NPV propagation at the $\tilde{z} = 0$ equator is evidently somewhat more pronounced in the case of the thinner ergosphere. It also noteworthy that the overall occurrence of NPV propagation is less common for the thinner ergosphere, as indicated by the generally lower NPV scores recorded in Figure 2 as compared with Figure 1.

^{||}If NPV occurs for both the k^+ and k^- wavenumbers for a particular (θ, ϕ) orientation then a score of two units was awarded.

From Figures 1 and 2 it is clear that the occurrence of NPV increases as the black hole rotation increases. It is therefore of interest to look at the scenario $a_{\text{rbh}} \rightarrow m_{\text{rbh}}$ for which the occurrence of NPV is maximized. The NPV distribution maps corresponding to $a_{\text{rbh}} = 0.99m_{\text{rbh}}$ are shown in Figure 3, for the same surfaces of constant R as were considered in Figures 1 and 2. In this maximized scenario, the regions which support NPV propagation are widely distributed throughout the ergosphere. However, we note the relative sparsity of NPV propagation in the vicinity of the black hole's axis of rotation.

Extrapolating from Figures 1, 2 and 3, we infer that NPV propagation does not occur

- (i) in neighbourhoods along the black hole's axis of rotation, and
- (ii) in the limit as the black hole's rate of rotation becomes vanishingly small.

We note that the outer event horizon and the stationary limit surface merge as the rotational rate approaches zero, and thereby the ergosphere disappears.

On comparing the maximum theoretical NPV score of 129600 with the maximum scores in Figures 1, 2 and 3, it is apparent that the conditions for NPV propagation are satisfied for relatively few wavevector orientations in the ergosphere. To illustrate this point further, we considered a single representative neighbourhood within the ergosphere, say $\tilde{x} = 0.2 m_{\text{rbh}}$, $\tilde{y} = 1.8 m_{\text{rbh}}$ and $\tilde{z} = 0.3 m_{\text{rbh}}$, with $a_{\text{rbh}} = m_{\text{rbh}} \sqrt{3/4}$ (for which $R = 1.63 m_{\text{rbh}}$). We computed $P_{a,b}$ for all orientations of $\hat{\underline{k}}$. At orientations where $P_{a,b} < 0$ a score of one unit was recorded. The scores are plotted against the spherical polar coordinates θ and ϕ of $\hat{\underline{k}}$ in Figure 4. Orientations at which $P_{a,b} < 0$ arises from the k^+ wavenumber are coloured red, whereas those orientations at which $P_{a,b} < 0$ occurs for the k^- wavenumber are coloured green. The k^+ NPV regions and the k^- NPV regions are observed in Figure 3 to occupy a relatively small portion of the (θ, ϕ) plane.

4 Concluding remarks

By using the Kerr metric in the Tamm formulation of electromagnetics in gravitationally affected vacuum, we have mapped the occurrence of negative-phase velocity (NPV) planewave propagation in the ergosphere of a rotating black hole. Our numerical results indicate that

- NPV propagation does not appear possible outside the stationary limit surface;
- rotation of a black hole is required for NPV propagation;
- NPV propagation is impossible on the axis of rotation of the black hole;
- regions of NPV propagation are concentrated at the equator of the ergosphere, and are less common towards the polar regions; and
- an increase in angular velocity exaggerates the NPV concentration at the equator.

In particular, the importance of the rotational character of the black hole metric should be stressed. In the absence of rotation the black hole metric does not support NPV propagation. The infeasibility of NPV propagation for (i) a non-rotating black hole; and (ii) along the axis of rotation of a black hole, is consistent with our earlier analytic results [5, 6]. In connection with this issue, we note that NPV propagation can however arise in Schwarzschild-de Sitter spacetime [20].

Let us comment upon the applicability of the NPV condition (47). Suppose that the neighbourhood \mathcal{R} has representative linear dimensions given by ρ . In order for the nonuniform metric $g_{\alpha\beta}$ to be approximated by the uniform metric $\tilde{g}_{\alpha\beta}$ throughout \mathcal{R} , it is necessary that ρ be small compared to the radius of curvature of the $g_{\alpha\beta}$ spacetime. A convenient measure of the inverse radius of spacetime curvature squared is provided by the nonzero components of the Riemann tensor. These components are of the order of R^{-2} for the Kerr metric [21]. Therefore, we have $\rho \ll R$. Since the neighbourhood \mathcal{R} is also required to be large compared with electromagnetic wavelengths, as given by $2\pi/|k|$, we see that (47) holds in the regime

$$\frac{2\pi}{|k|} \ll R. \quad (51)$$

For black holes of the mass of our sun, the condition (51) translates to wavelengths of the order of 100 metres or less, whereas for supermassive black holes of the type believed to lie at the centre of galaxies the NPV condition (47) holds for wavelengths of the order of 10^7 kilometres or less, typically [22].

The NPV phenomenon reported in the preceding sections concerns the propagation of electromagnetic plane waves in the ergosphere. The issue of possible generalizations to scalar and/or gravitational waves is a matter for future study. However, we note in this context that the Teukolsky equation yields general (nonplanar) solutions which support negative wavenumbers for scalar, electromagnetic and gravitational waves in the ergosphere of a Kerr black hole [23]–[25].

It is of interest to speculate whether the NPV propagation demonstrated here may arise for so-called acoustic black holes [26], typically studied in the cylindrical geometry [27]. While cylindrical acoustic black holes can support superradiant scattering analogously to the equatorial slice of the Kerr black hole [27, 28], the propagation of NPV acoustic waves for acoustic black holes has yet to be established.

We close by emphasizing that the description of NPV presented herein arises from the classical treatment of electromagnetic waves in curved spacetime, within the short wavelength regime indicated by (51). This NPV phenomenon is distinct from superradiant scattering in the ergosphere at long wavelengths [29].

Acknowledgement

SS acknowledges EPSRC for support under grant GR/S60631/01. We thank two anonymous referees for comments that helped us improve this communication.

References

- [1] Lakhtakia A, McCall M W, and Weiglhofer W S 2002 Brief overview of recent developments on negative phase-velocity mediums (alias left-handed materials) *AEÜ Int. J. Electron. Commun.* **56** 407–410
- [2] Lakhtakia A, McCall M W, and Weiglhofer W S 2003 Negative phase-velocity mediums *Introduction to Complex Mediums for Optics and Electromagnetics* ed WS Weiglhofer and A Lakhtakia (Bellingham, WA, USA: SPIE Press) pp347–363
- [3] Pendry J B 2004 Negative refraction *Contemp. Phys.* **45** 191–202
- [4] Shelby R A, Smith D R and Schultz S 2001 Experimental verification of a negative index of refraction *Science* **292** 77–79
- [5] Lakhtakia A and Mackay T G 2004 Towards gravitationally assisted negative refraction of light by vacuum *J. Phys. A: Math. Gen.* **37** L505–L510; corrigendum 2004 **37** 12093
- [6] Lakhtakia A, Mackay T G and Setiawan S 2005 Global and local perspectives of gravitationally assisted negative-phase-velocity propagation of electromagnetic waves in vacuum *Phys. Lett. A* **336** 89–96
- [7] Landau L D and Lifshitz E M 1975 *The Classical Theory of Fields* (Oxford, UK: Clarendon Press) §90
- [8] Skrotskii G V 1957 The influence of gravitation on the propagation of light *Soviet Phys.-Dokl.* **2** 226–229
- [9] Plebanski J 1960 Electromagnetic waves in gravitational fields *Phys. Rev.* **118** 1396–1408
- [10] Møller C 1972 *The Theory of Relativity* 2nd ed. (Oxford, UK: Clarendon Press)
- [11] Mashhoon B 1973 Scattering of electromagnetic radiation from a black hole *Phys. Rev. D* **7** 2807–2814
- [12] Schleich W and Scully M O 1984 General relativity and modern optics *New Trends in Atomic Physics* ed G Grynberg and R Stora (Amsterdam, Holland: Elsevier Science Publishers) pp995–1124
- [13] Burko L M 2002 Self-interaction near dielectrics *Phys. Rev. E* **65** 046618
- [14] Mackay T G, Lakhtakia A and Setiawan S 2005 Gravitation and electromagnetic wave propagation with negative phase velocity *New J. Phys.* **7** 75
- [15] Kerr R P 1963 Gravitational field of a spinning mass as an example of algebraically special metrics *Phys. Rev. Lett.* **11** 237–238

- [16] Chen H C 1983 *Theory of Electromagnetic Waves* (New York, USA: McGraw–Hill)
- [17] d’Inverno R 1992 *Introducing Einstein’s Relativity* (Oxford, UK: Clarendon Press) Chap 19
- [18] Lakhtakia A 1992 General schema for the Brewster conditions *Optik* **90** 184–186
- [19] Mackay T G and Lakhtakia A 2004 Negative phase velocity in a uniformly moving, homogeneous, isotropic, dielectric–magnetic medium *J. Phys. A: Math. Gen.* **37** 5697–5711
- [20] Mackay T G, Lakhtakia A and Setiawan S 2005 Electromagnetic waves with negative phase velocity in Schwarzschild-de Sitter spacetime *Europhys. Lett.* (accepted for publication)
- [21] Chandrasekhar S 1983 *The Mathematical Theory of Black Holes* (Oxford, UK: Clarendon Press)
- [22] New K C B and Shapiro S L 2001 The formation of supermassive black holes and the evolution of supermassive stars *Class. Quantum Grav.* **18** 3965–3975
- [23] Teukolsky S A 1973 Perturbations of a rotating black hole. I Fundamental equations for gravitational electromagnetic, and neutrino–field perturbations *Astrophys. J.* **185** 635–647
- [24] Press W H and Teukolsky S A 1973 Perturbations of a rotating black hole. II Dynamical stability of the Kerr metric *Astrophys. J.* **185** 649–673
- [25] Teukolsky S A and Press W H 1974 Perturbations of a rotating black hole. III Interaction of the hole with gravitational and electromagnetic radiation *Astrophys. J.* **193** 443–461
- [26] Barceló C, Liberati S, Sonogo S and Visser M 2004 Causal structure of analogue spacetimes *New J. Phys.* **6** 186
- [27] Visser M 1998 Acoustic black holes: horizons, ergospheres and Hawking radiation *Class. Quant. Grav.* **15** 1767–1791
- [28] Berti E 2005 Black holes in a bath tub *J. Phys.: Conf. Series* **8** 101–105
- [29] Setiawan S, Mackay T G and Lakhtakia A 2005 A comparison of superradiance and negative–phase–velocity phenomena in the ergosphere of a rotating black hole *Phys. Lett. A* **341** 15–21

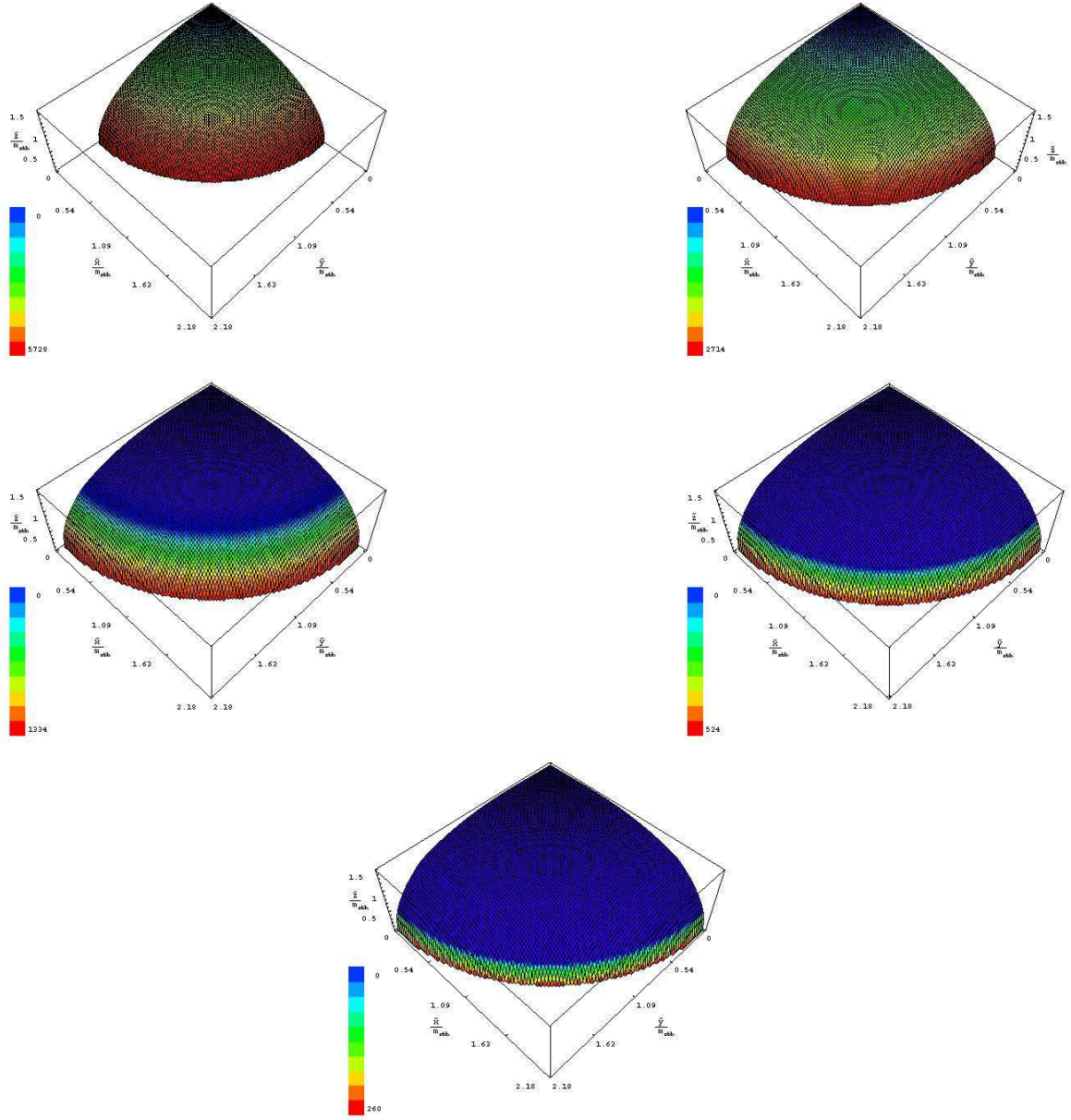


Figure 1: NPV maps for $a_{\text{rbh}} = m_{\text{rbh}}\sqrt{3/4}$. See the text for an explanation of the colour mapping. (a) At the surface $R = R_+$ (i.e., at the outer event horizon)(top left); (b) At the surface $R = 0.5R_+ + 0.5R_{S_+}$ (top right); (c) At the surface $R = 0.25R_+ + 0.75R_{S_+}$ (middle left); (d) At the surface $R = 0.1R_+ + 0.9R_{S_+}$ (middle right); and (e) At the surface $R = 0.05R_+ + 0.95R_{S_+}$ (bottom) .

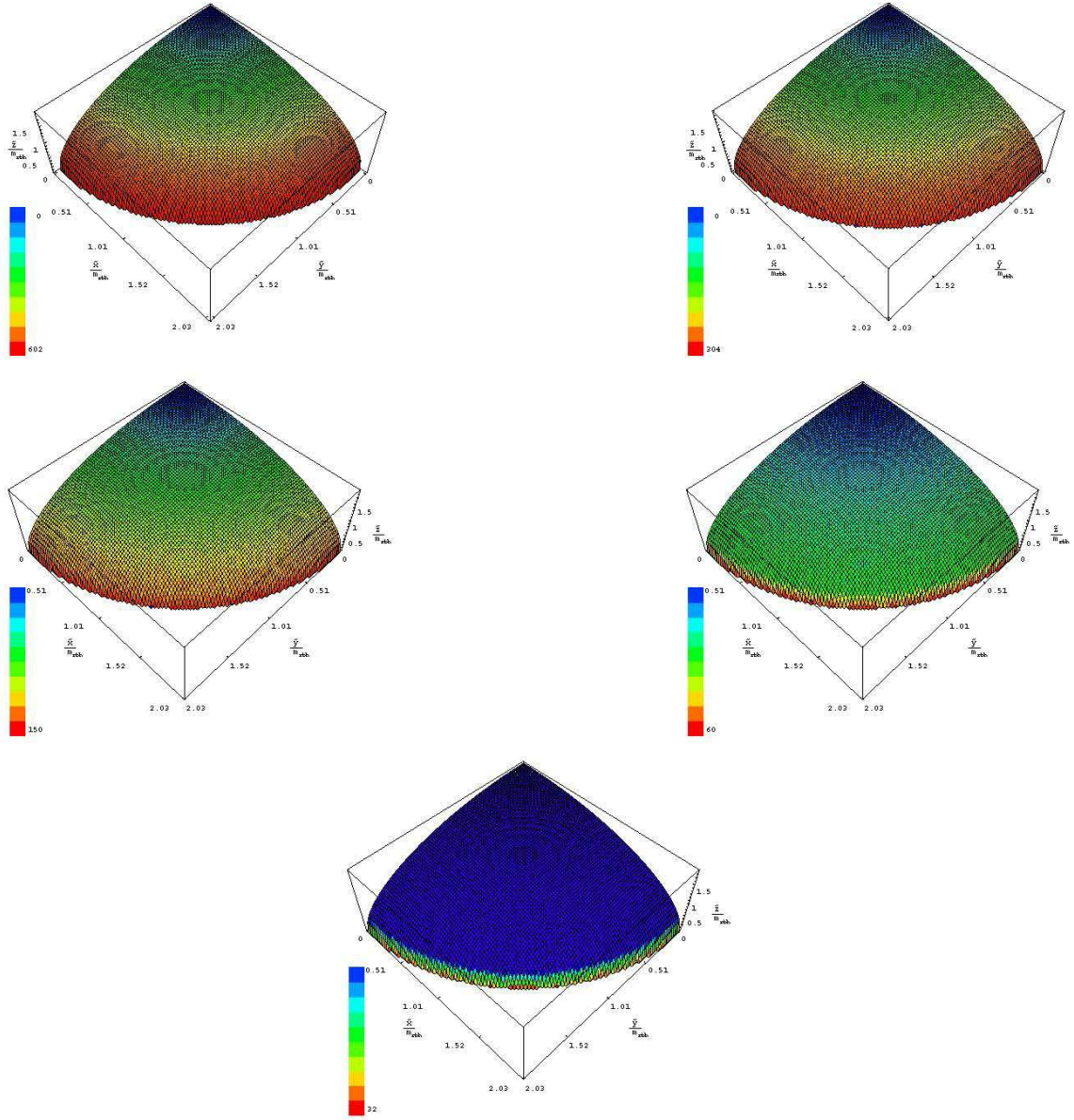


Figure 2: NPV maps for $a_{\text{rbh}} = m_{\text{rbh}}/3$. See the text for an explanation of the colour mapping. (a) At the surface $R = R_+$ (i.e., at the outer event horizon) (top left); (b) At the surface $R = 0.5R_+ + 0.5R_{S_+}$ (top right); (c) At the surface $R = 0.25R_+ + 0.75R_{S_+}$ (middle left); (d) At the surface $R = 0.1R_+ + 0.9R_{S_+}$ (middle right); and (e) At the surface $R = 0.05R_+ + 0.95R_{S_+}$ (bottom).

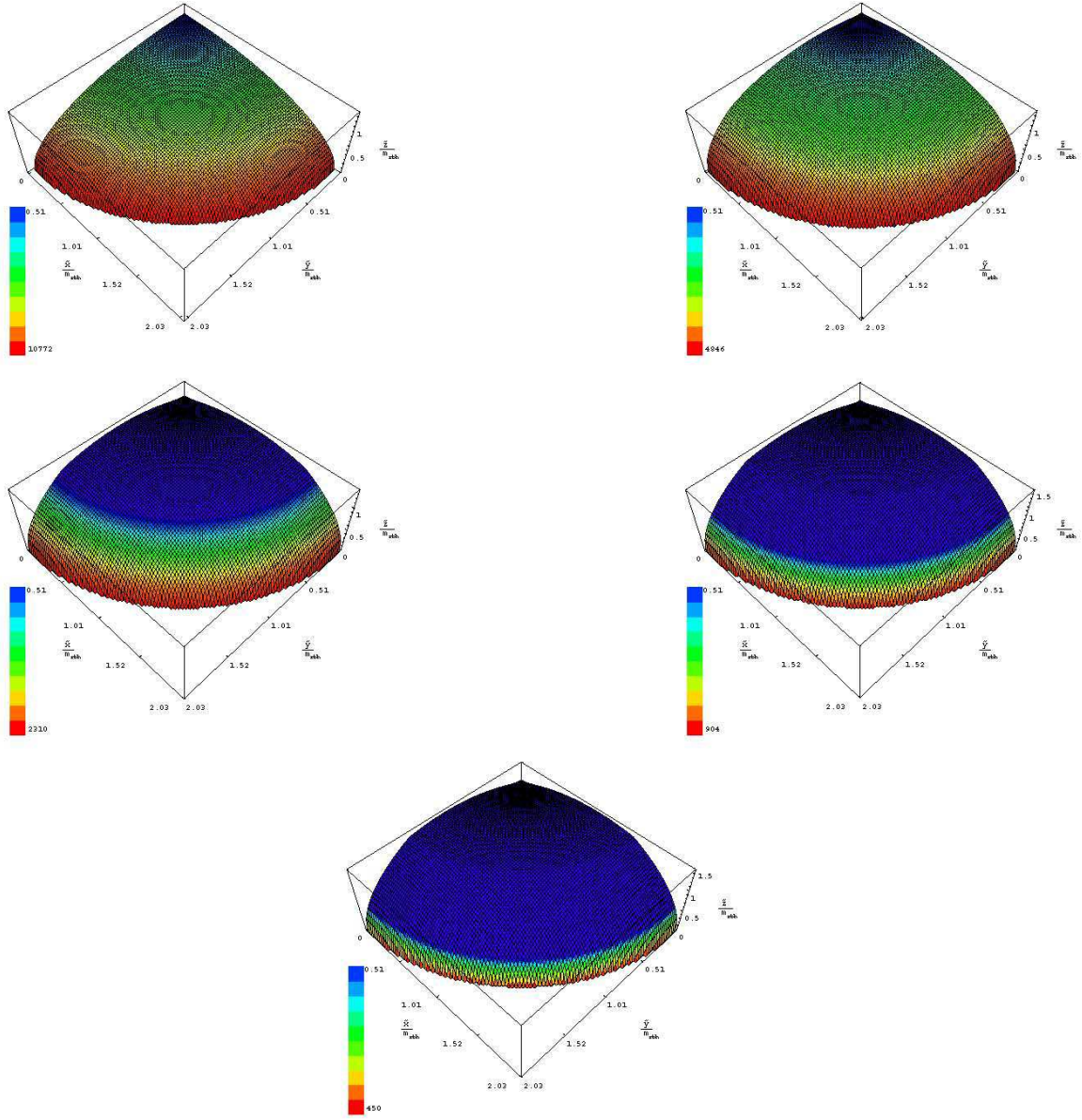


Figure 3: NPV maps for $a_{\text{rbh}} = 0.99m_{\text{rbh}}$. See the text for an explanation of the colour mapping. (a) At the surface $R = R_+$ (i.e., at the outer event horizon) (top left); (b) At the surface $R = 0.5R_+ + 0.5R_{S_+}$ (top right); (c) At the surface $R = 0.25R_+ + 0.75R_{S_+}$ (middle left); (d) At the surface $R = 0.1R_+ + 0.9R_{S_+}$ (middle right); and (e) At the surface $R = 0.05R_+ + 0.95R_{S_+}$ (bottom).

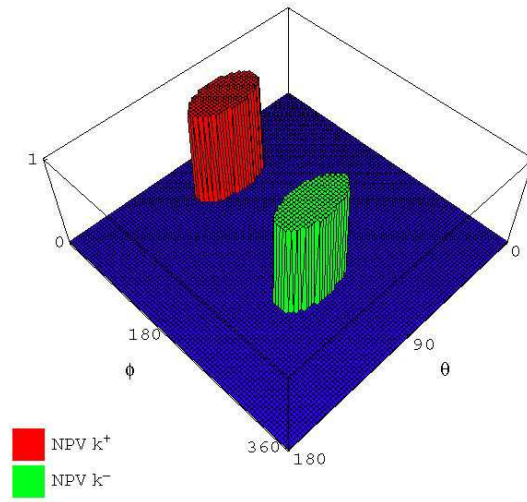


Figure 4: NPV scores plotted as heights, against the \hat{k} orientational angles θ and ϕ , in the neighbourhood of $(\tilde{x} = 0.2 m_{\text{rbh}}, \tilde{y} = 1.8 m_{\text{rbh}}, \tilde{z} = 0.3 m_{\text{rbh}})$, with $a_{\text{rbh}} = m_{\text{rbh}} \sqrt{3/4}$. NPV arising from the k^+ wavenumber is coded red; NPV arising from the k^- wavenumber is coded green.